VOLUME 98 | NUMBER 2 | OCTOBER 2015 | ISSN 0950-382X | www.mol-micro.com

molecular microbiology

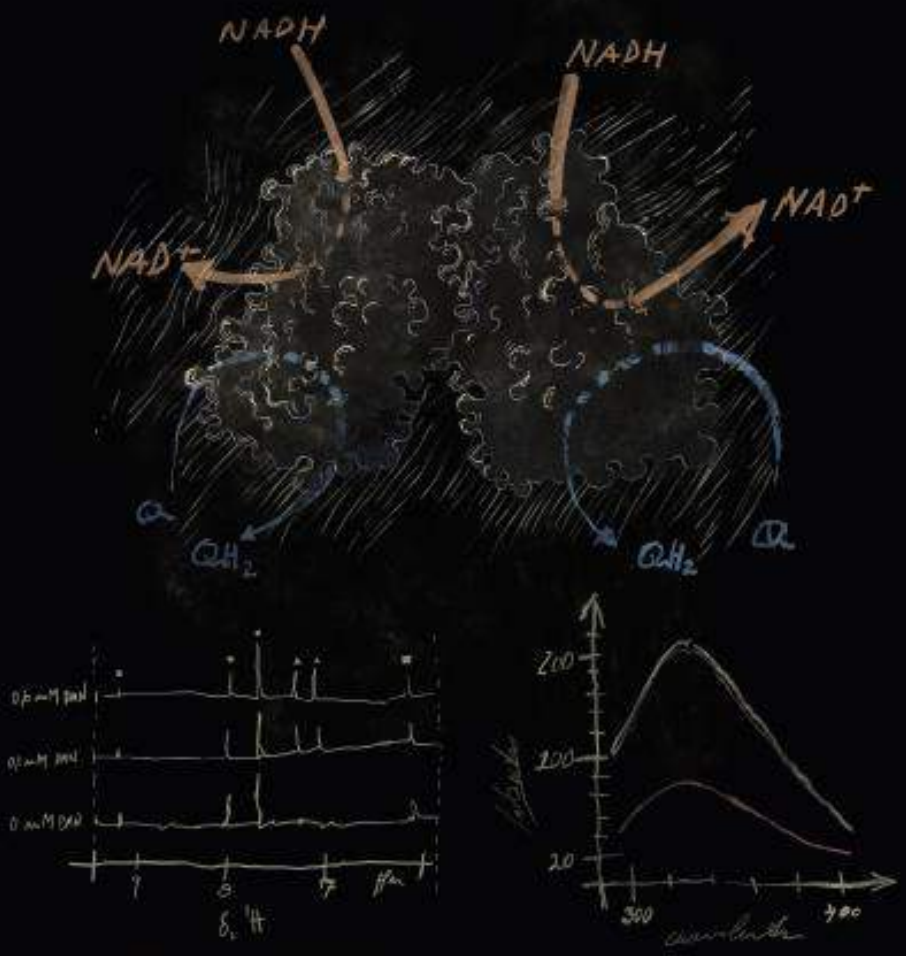

On the cover:
Protein-substrate interactions in *Staphylococcus aureus* NDH-2

Pleiotropic effects of SuhB, a ribosome-associated protein that modulates ribosome stalling

Mechanisms of repression by the *Escherichia coli* DsrA regulatory RNA

Bacillithiol and Fe-S cluster biogenesis in *S. aureus*

WILEY Blackwell

Molecular Microbiology (2015) 98(2), 272–288 ■
doi:10.1111/mmi.13120
First published online 30 July 2015

Type-II NADH:quinone oxidoreductase from *Staphylococcus aureus* has two distinct binding sites and is rate limited by quinone reduction

Filipa V. Sena,[1] Ana P. Batista,[1] Teresa Catarino,[1,2] José A. Brito,[1] Margarida Archer,[1] Martin Viertler,[3] Tobias Madl,[3] Eurico J. Cabrita[4] and Manuela M. Pereira[1]*

[1]*Instituto de Tecnologia Química e Biológica – António Xavier, Universidade Nova de Lisboa, Av. da República EAN, 2780-157, Oeiras, Portugal.*

[2]*Departamento de Química, Faculdade de Ciências e Tecnologia, Universidade Nova de Lisboa, 2829-516, Caparica, Portugal.*

[3]*Center for Integrated Protein Science Munich (CIPSM) at the Department of Chemistry Technische Universität München, Lichtenbergstr.4, 85747 Garching, Germany and Institute of Structural Biology, Helmholtz Zentrum München Neuherberg and Biomolecular NMR-Spectroscopy,* and *Institute of Molecular Biology & Biochemistry, Center of Molecular Medicine, Medical University of Graz, 8010, Graz, Austria.*

[4]*REQUIMTE, UCIBIO, Departamento de Química, Faculdade de Ciências e Tecnologia, Universidade Nova de Lisboa, 2829-516, Caparica, Portugal.*

Summary

A prerequisite for any rational drug design strategy is understanding the mode of protein–ligand interaction. This motivated us to explore protein–substrate interaction in Type-II NADH:quinone oxidoreductase (NDH-2) from *Staphylococcus aureus*, a worldwide problem in clinical medicine due to its multiple drug resistant forms. NDHs-2 are involved in respiratory chains and recognized as suitable targets for novel antimicrobial therapies, as these are the only enzymes with NADH:quinone oxidoreductase activity expressed in many pathogenic organisms.

We obtained crystal and solution structures of NDH-2 from *S. aureus*, showing that it is a dimer in solution. We report fast kinetic analyses of the protein and detected a charge-transfer complex formed between NAD^+ and the reduced flavin, which is dissociated by the quinone. We observed that the quinone reduction is the rate limiting step and also the only half-reaction affected by the presence of HQNO, an inhibitor. We analyzed protein–substrate interactions by fluorescence and STD-NMR spectroscopies, which indicate that NADH and the quinone bind to different sites.

In summary, our combined results show the presence of distinct binding sites for the two substrates, identified quinone reduction as the rate limiting step and indicate the establishment of a NAD^+-protein complex, which is released by the quinone.

Accepted 6 July, 2015. *For correspondence. E-mail: mpereira@itqb.unl.pt; Tel. +351-214469312; Fax +351-214469314.

Introduction

The rise of multidrug-resistant bacteria has prompted the search for new targets for antibiotic action. Type-II NADH:quinone oxidoreductases (NDH-2) are promising new targets for antibiotics (Weinstein *et al.*, 2005; Lin *et al.*, 2011; Biagini *et al.*, 2012; Farha *et al.*, 2013; Cook *et al.*, 2014). NDH-2 are membrane proteins involved in respiratory chains, absent in mammals and the only NADH:quinone oxidoreductases expressed in some pathogenic microorganisms, as in the case of *Staphylococcus aureus*, one of the most common causes of clinical infections. Multidrug-resistant staphylococci particularly methicillin-resistant *S. aureus* (MRSA) pose a growing problem for human health, both in the treatment and control of infections (Brumfitt and Hamilton-Miller, 1990; Salgado-Pabon and Schlievert, 2014).

Furthermore, NDHs-2 performs the same catalytic function as the respiratory complex I and thus the potential use of NDH-2 has been suggested in gene therapy correcting NADH:quinone oxidoreductase activity in pathologies with malfunctioning Complex I, such as neurodegenerative disorders, including Parkinson's disease and aging (Schapira, 1998; Dawson and Dawson, 2003). It has been observed that NDH-2 expression restores the mitochondrial activity in animals with complex I deficiency (Yagi *et al.*, 2006).

All NDHs-2 share the same domain organization containing two typical dinucleotide binding domains, both harboring a conserved GxGxxG motif. One of these motifs

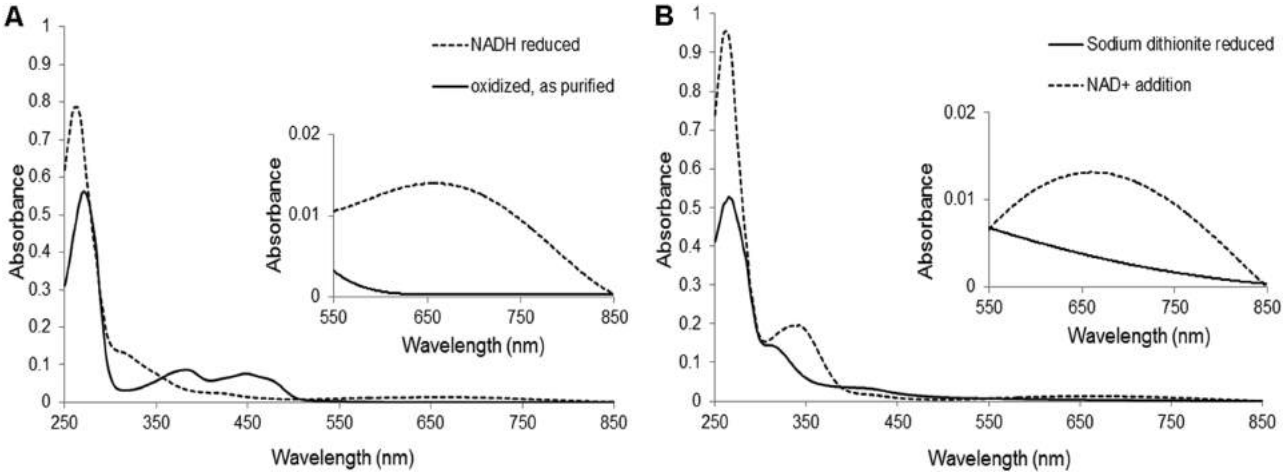

Fig. 1. UV-visible absorption spectra of NDH-2 from *S. aureus*.
A. NDH-2 as purified (solid line) and reduced with NADH (dashed line). The inserted figure expands absorption spectrum in the 600–800 nm region.
B. NDH-2 reduced with dithionite (solid line) and incubated with NAD^+ (dashed line). The inserted figure expands absorption spectrum in the 600–800 nm region.

binds flavin adenine dinucleotide (FAD), the only prosthetic group, whereas the other interacts with NADH (Kerscher, 2000). The study of NDH-2 gained a new impetus after the publication of two crystal structures of NDH-2 from *Saccharomyces cerevisiae* (Ndi1) (Feng *et al.*, 2012; Iwata *et al.*, 2012). These studies prompted further discussions including the number and location of the substrate binding sites. The work by Iwata *et al.* (2012) discussed overlapping binding sites for NADH and quinone, whereas Feng *et al.* (2012) proposed separated binding sites at opposite sides of the isoalloxazine ring of FAD. In the first crystal structure of a bacterial NDH-2 enzyme, recently reported by Heikal *et al.* (2014), binding sites for NADH and quinone could be modeled as proposed by Feng *et al.*, suggesting the existence of distinct binding sites for the two substrates.

A number of studies analyzing the kinetic properties of the NDHs-2 from *Yarrowia lipolytica* (Eschemann *et al.*, 2005), *Mycobacterium tuberculosis* (Yano *et al.*, 2006) and *S. cerevisiae* (Velazquez and Pardo, 2001; Yamashita *et al.*, 2007) have indicated that these enzymes operate by a ping-pong mechanism. Those studies suggested the existence of only one binding site. A recent study of NDH-2 from *M. tuberculosis* proposed a non-classical, two-site ping-pong kinetic mechanism where quinone binds to a site different from the NADH binding site (Yano *et al.*, 2014). In contrast, Yang *et al.* concluded that the reaction proceeds through the establishment of a ternary complex (Yang *et al.*, 2011). Recently two putative NDH-2 from *S. aureus* were biochemical characterized and the inhibitory effects of phenothiazines were investigated (Schurig-Briccio *et al.*, 2014).

In this work, we explore the interaction of NDH-2 from *S. aureus* with substrates and present its thorough biochemical, structural and functional characterization. This investigation aims to provide the basis of a possible approach to rational drug design.

Results

Biochemical characterization

NDH-2 from *S. aureus* was expressed and purified from the membranes of *Escherichia coli* as previously reported (Rosario *et al.*, 2015). NDH-2 presented an absorption spectrum typical of a flavoprotein, exhibiting bands with maxima at 375 and 450 nm and a shoulder close to 475 nm (Fig. 1A). The flavin cofactor, identified as flavin adenine dinucleotide (FAD) by HPLC analysis, is non-covalently bound as it could be removed by acidic precipitation or thermal denaturation. One molecule of FAD was present per molecule of protein, and the presence of other compounds, such as quinones, was not observed. The reduction potential of FAD, determined by cyclic voltammetry, is -222 ± 20 mV *vs* SHE, which is in the range typical of flavin cofactors (Edwards, 2014). The thermal denaturation profile of NDH-2 monitored by the change in fluorescence of FAD shows a transition at approximately 55°C (Fig. S1), indicating that NDH-2 maintains its FAD up to 50°C.

The fully reduced state of NDH-2 was achieved under anaerobic conditions by incubation with NADH. NDH-2 reduction is characterized by the loss of absorption in the 375–450 nm region and appearance of a broad absorp-

tion band with maximum at 650–800 nm (Fig. 1A). Further incubation with 2,3-Dimethyl-1,4-naphthoquinone (DMN) reoxidized the protein, leading to the reappearance of absorption in the 375–450 nm region and disappearance of that in the 650–800 nm region. A fully reduced state of NDH-2 was also obtained using sodium dithionite, and a loss of absorption in the 375–450 nm region was also observed, but the absorption in the 650–800 nm region was not detected (Fig. 1B). The absorption in the latter region could be restored by adding NAD^+ to the dithionite-reduced NDH-2 (Fig. 1B). This observation shows that the absorption in the 650–800 nm region indicates the presence of NAD^+ bound to the reduced protein.

Structural studies

The crystal structure of NDH-2 from *S. aureus* (PDB entry 4XDB) was solved by molecular replacement using the co-ordinates of the homologue from *Caldalkalibacillus thermarum* (PDB 4NWZ) (Heikal *et al.*, 2014). The structure was refined to 3.32 Å with R_{cryst} of 20.4% and R_{free} of 24.9%, data collection and refinement statistics are depicted in Table 1. The final crystallographic model comprises four monomers (amino acid residues Gln3 or Lys6 to Phe402, depending on the monomer), four FAD molecules, six chloride ions and 77 water molecules. The NDH-2 overall fold is composed of two Rossmann-like domains and a C-terminal domain (Fig. 2A and B). The first domain, or FAD binding domain, comprises residues 3–114 and 265–349 and binds non-covalently the FAD group that is present in an extended conformation. The second domain is the NADH-binding domain and includes residues 115–264. These two domains compose the canonical fold for the glutathione-reductase family of flavin-containing enzymes. The C-terminal, or membrane attachment domain, comprising residues 350–402, is constituted by an anti-parallel three-stranded β-sheet followed by two helices arranged in a helix-turn-helix motif.

The most similar structures to *S. aureus* NDH-2 are those of *C. thermarum* NDH-2 (PDB 4NWZ) (Heikal *et al.*, 2014) and *S. cerevisiae* Ndi [PDB entries 4G6G and 4G9K (Feng *et al.*, 2012; Iwata *et al.*, 2012)] showing RMSDs of 1.2 Å and 2.4 Å for the aligned C_α atoms and sharing 46% and 27% of sequence identity respectively (Fig 3). Sulfide:quinone oxidoreductases [e.g. SQRs from *Acidithiobacillus ferroxidans* (PDB 3T2Y; Cherney *et al.*, 2012), *Aquifex aeolicus* (PDB 3HYW; Marcia *et al.*, 2009) and *Acidianus ambivalens* (PDB 3H8L; Brito *et al.*, 2009)] show the same overall fold with RMSDs of ~ 2.4 Å for 360 aligned C_α atoms.

The electrostatic surface potential (Fig. 2C and D) displays a hydrophobic surface surrounded by two patches of positively charged residues at the C-terminus, as previously reported for *C. thermarum* NDH-2 and *S. cerevisiae* Ndi1 (Feng *et al.*, 2012; Iwata *et al.*, 2012; Heikal *et al.*, 2014). These patches are important to establish interactions with the negatively charged head of the phospholipids, whereas the adjacent hydrophobic surface comprised mainly by phenylalanine residues within the helix-turn-helix motif is more buried within the membrane.

Similar to the aforementioned structures, *S. aureus* NDH-2 also presents a cleft formed by residues Phe116, Ile118, Thr233-Ile235, Trp261-Gly263, Pro317 and Thr318 that leads to the *re*-side of FAD, which should be the NADH-binding site (Fig. 4A). These amino acid residues are highly conserved among the reported 3D-structures of NDH-2 (Feng *et al.*, 2012; Iwata *et al.*, 2012; Heikal *et al.*, 2014). Moreover, the turn Val163-Gly170 is also suggested to be involved in NADH binding by Heikal *et al.* (2014). Here the bulkier side-chain of phenylalanine in bacterial NDH-2 (Phe168 in *S. aureus* in contrast to Pro238 in *S. cerevisiae*) causes some steric constraints in the pocket where the NADH nicotinamide moiety stacks against the FAD isoalloxazine ring. This implies a slight structural rearrangement of Phe168 upon NADH binding.

Table 1. Data collection and refinement statistics for the structure of NDH-2 from *S. aureus*.

Data collection	
Wavelength (Å)	0.873
Resolution (Å)*	60.5 – 3.32 (3.33 – 3.32)
Space group	$P2_12_12_1$
a, b, c (Å)	81.78, 86.03, 269.95
α, β, γ (°)	90, 90, 90
R_{pim}	0.09 (0.36)
R_{merge}	0.15 (0.49)
$CC_{1/2}$	0.98 (0.72)
$\langle I/\sigma(I)\rangle$	8.3 (2.0)
Completeness (%)	99.5 (90.4)
Redundancy	3.6 (2.3)
No. reflections	104532 (617)
No. of unique reflections	28851 (264)
Wilson B factor (Å^2)	60.46
Refinement	
R_{cryst} (%)	20.4 (26.3)
R_{free} (%)	24.9 (31.3)
RMSD bond lengths (Å)	0.003
RMSD bond angles (°)	0.724
No. of protein atoms	12298
No. of ligand/ion atoms	218
No. of water atoms	77
Average protein *B*-factor (Å^2)	55.89
Average ligand/ion *B*-factor (Å^2)	44.64
Average water *B*-factor (Å^2)	39.27
Ramachandran plot statistics (%)	
Favoured regions	95.0
Allowed regions	4.2
Outliers	0.8
PDB entry	4XDB

* Values in parentheses refer to the highest resolution shell.

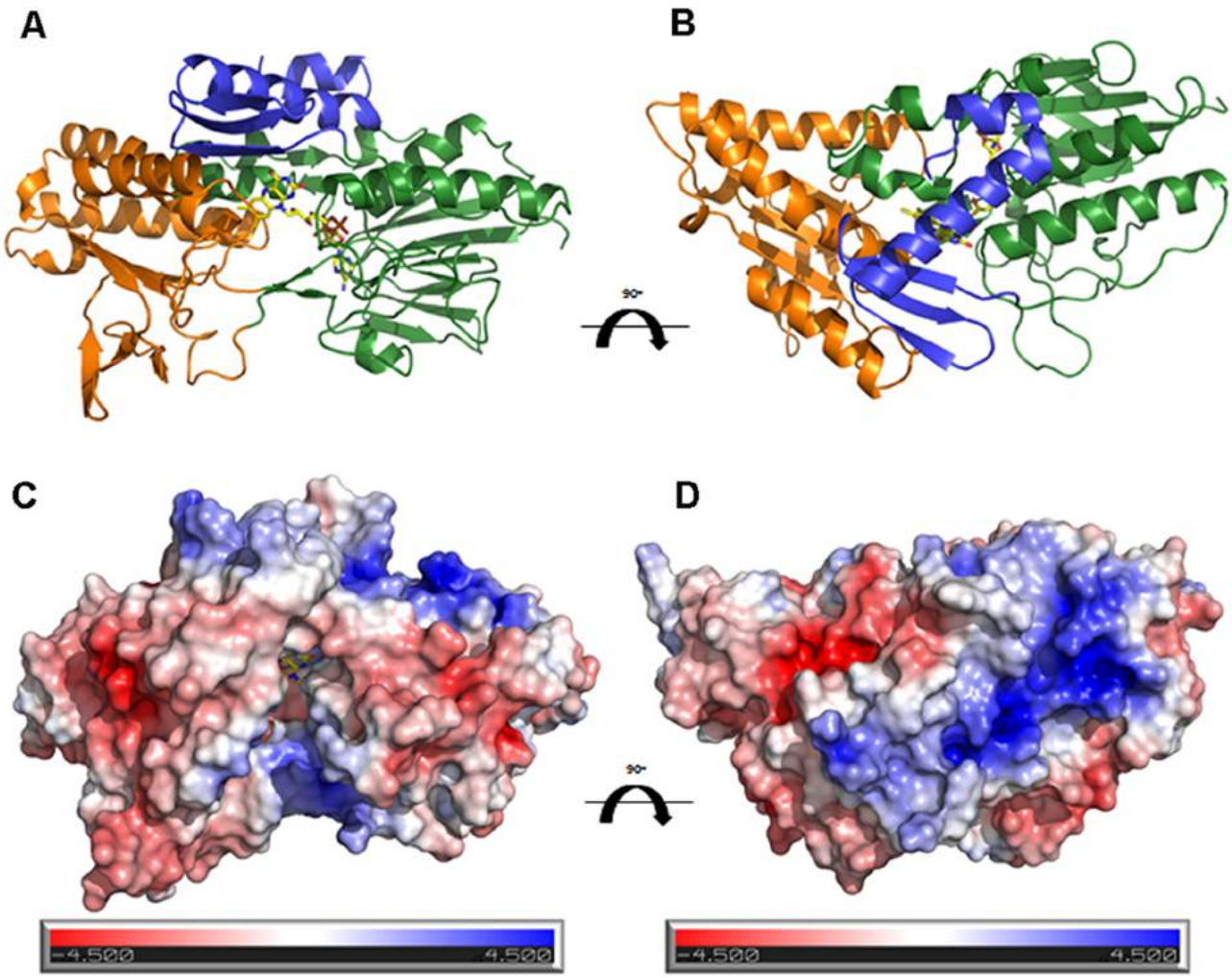

Fig. 2. Crystal structure of *S. aureus* NDH-2.
A. Cartoon representation of NDH-2 monomer from *S. aureus*; NADH-binding domain is colored in orange, FAD-binding domain in green and membrane attachment (C-terminal) domain in blue; FAD cofactor is shown in sticks with carbon atoms colored in yellow, oxygen in red and nitrogen in blue.
B. NDH-2 as viewed from the membrane (90° rotation relative to A); color code as in A.
C and D. Electrostatic surface potential of NDH-2 in the same orientations as in (A) and (B) (± 4.5 kT/e).

Staphylococcus aureus NDH-2 contains a tunnel that gives access to the *si*-side of FAD and is lined mostly by hydrophobic residues, namely Tyr15, Ala319, Met323, Ile382 and Ala386, also including the 319-AQxAxQ-324 motif proposed to characterize the quinone binding site (Heikal *et al*., 2014). The hydrophobic feature of this cavity as well as the AQxAxQ motif is maintained in the other NDH-2 structures (Fig. 4B). Interestingly, a quinone was observed to bind in this cavity in the *S. cerevisiae* Ndi1 reported by Feng *et al*. (2012), in contrast to the one reported by Iwata *et al*. (2012), where the quinone and NADH binding sites overlap on the *re*-side of FAD. Upon superposition with the *S. cerevisiae* Ndi1 structure with the two substrates present (Feng *et al*., PDB code 4G73), it is clear that *S. aureus* NDH-2 can accommodate a

Fig. 3. Superposition of NDH-2s. X-ray structures from NDH-2 from *S. aureus* (in yellow), *C. thermarum* (in lighter gray, PDB 4NWZ) and Ndi1 from *S. cerevisiae* (in darker gray, PDB 4G9K) with FAD in CPK mode.

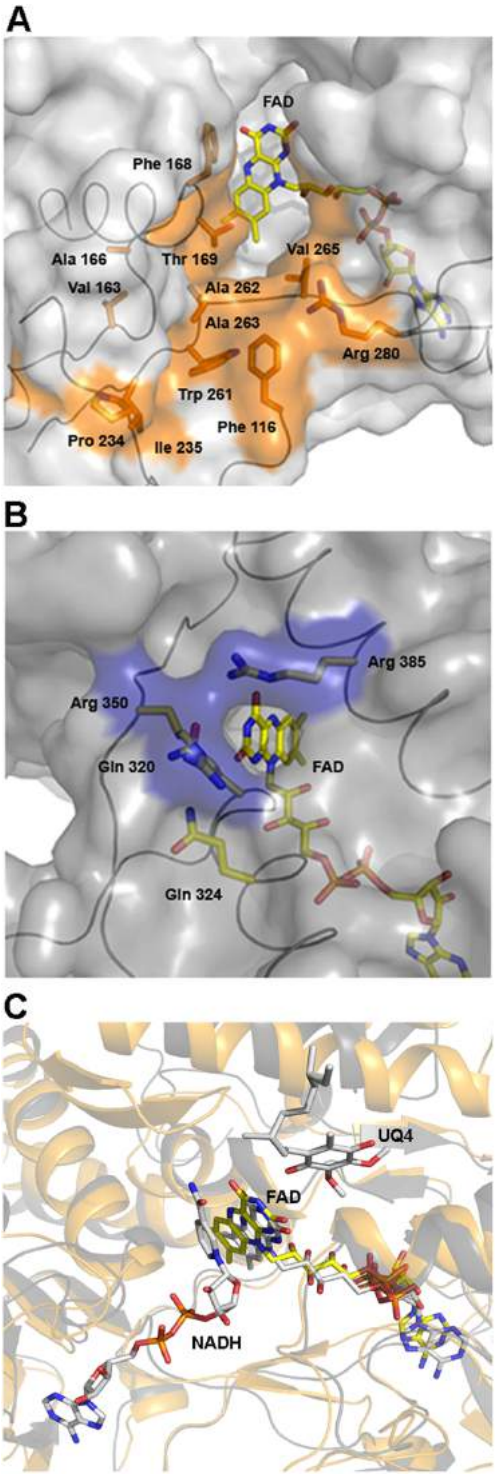

Fig. 4. Ligand binding sites around FAD.
A. NADH-binding cleft; surface representation with relevant residues for NADH-binding in orange.
B. Putative quinone binding site; surface with important residues in blue; Arg350 and Arg385 at the pocket entrance and Gln320 and Gln324 from AQxAxQ motif.
C. superposing (with FAD cofactors) of NDH-2 from *S. aureus* (in yellow) and Ndi1 from *S. cerevisiae* (in gray, PDB 4G73) structures, showing the NADH and ubiquinone-4 (UQ_4) in sticks bound to it (PDB 4G73).

quinone in the cavity described above (Fig. 4B). This cavity is delineated by Val353, Val365, Phe366, Ile370 and Met378, similarly to *C. thermarum* structure (Heikal *et al.*, 2014). Conformational rearrangements would be necessary for the quinone to surpass the FAD moiety in order to bind at the same site as the NADH, as proposed by Iwata *et al.*, which does not seem likely (Fig. 4C). Two arginine residues, Arg350 and Arg385, are located at the tunnel entrance showing high thermal displacement parameters (B-factor around 80 $Å^2$), which suggest flexibility on their side-chains.

The crystal asymmetric unit of *S. aureus* NDH-2 contains 4 polypeptide chains packed as two nearly identical homodimers (Fig. S2). The dimeric interface is mainly hydrophilic and has a buried area around 1,076 $Å^2$ per monomer, corresponding to ca. 6% of the total solvent-accessible area as assessed by PISA (Krissinel and Henrick, 2007). Most of the polar and charged residues (Arg, Lys and Glu) present at the interface are located in a long stretch just before the C-terminal membrane attachment domain. This arrangement is not physiologically relevant as the C-terminal membrane domains of both monomers face each other and shield some hydrophobic residues from the solvent; this architecture of dimerization makes the membrane domains to pack against their counterpart from the neighboring monomer and hence inaccessible for membrane attachment (Fig. S2).

Given that the dimer interfaces for previously reported homologous structures differ significantly (Iwata *et al.*, 2012; Heikal *et al.*, 2014), we set off to characterize the conformation of *S. aureus* NDH-2 in solution using small-angle X-ray scattering (SAXS). We found that, in agreement with size exclusion chromatography (Fig. S3), NDH-2 is a dimer in solution (maximal dimension (D_{max}): 110 Å, radius of gyration (R_g): 34 ± 1, Molecular mass 93 kDa) (Fig. 5). To evaluate whether any of the reported dimer orientations match the SAXS data of *S. aureus* NDH-2, we compared SAXS data back-calculated from crystal structures of the homologous proteins from *C. thermarum* (4NWZ) and *S. cerevisiae* (4G9K). Clearly, neither of the dimer orientations of these two crystal structures was in good agreement with the data obtained for *S. aureus* (Fig. 5A). In *S. cerevisiae* Ndi1, the dimer interface includes a long C-terminal helix, which is not present in the bacterial homologues. Furthermore, due to the lack of solution studies of the homologous proteins, we cannot exclude that the different dimer orientation observed in the crystal structures might be due to crystal packing forces. Thus, the observed difference may reflect different orientations of the monomers, or an equilibrium between different conformations. Indeed, a superposition of SAXS data back-calculated for the two homologous proteins and assuming a population ratio of 40:60% (*C. thermarum*:*S. cerevisiae*) resulted in good agreement with the

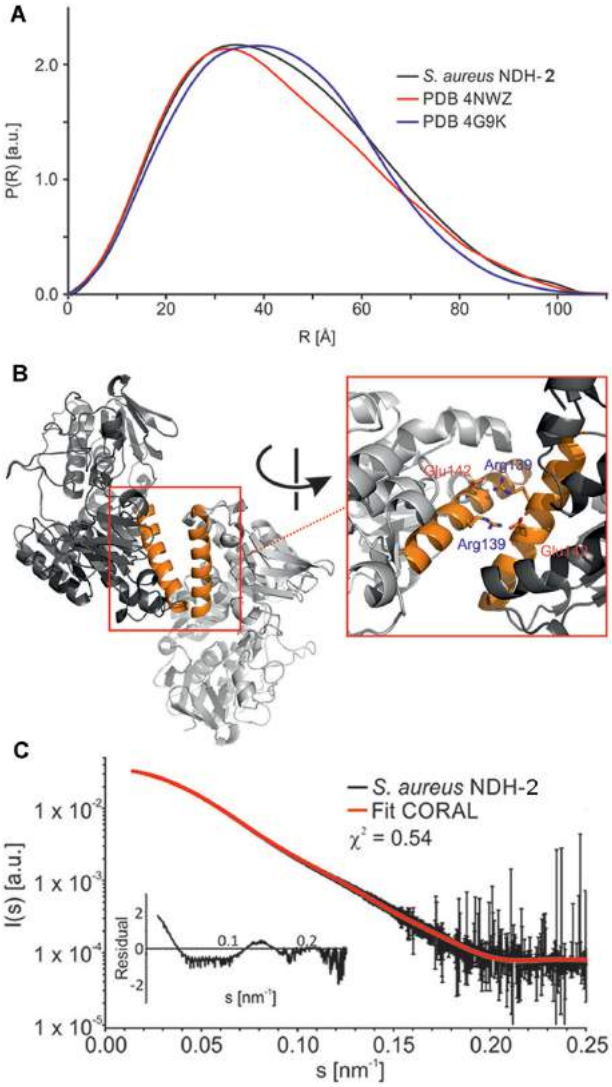

Fig. 5. SAXS Measurements.
A. Comparison of SAXS radial density distributions of NDH-2 from *S. aureus* (experimental data), *Caldalkalibacillus thermarum* NDH-2 (back-calculated from PDB 4NWZ) and *Saccharomyces cerevisiae* (back-calculated from PDB 4G9K). The P(R) of the physiologically relevant dimer orientations is shown. Neither of the other dimer interfaces observed in the crystal structures yielded an acceptable agreement ($\chi 2$ between 3.1 and 12.0).
B. SAXS rigid body model of NDH-2 from *S. aureus*. Residues in the dimerization interface forming salt bridges are labeled.
C. Comparison of experimental NDH-2 from *S. aureus* SAXS data with SAXS data back-calculated from the CORAL model of the dimer of NDH-2 from *S. aureus*. I(s) axis is shown in a logarithmic representation. The angular ranges from 0.0012–0.25 nm^{-1} are compared.

experimental data (Fig. S4). To test whether a single, though different, conformation compared with the crystal structures of the homologous proteins could explain the SAXS data, we carried out rigid body modeling of the dimeric *S. aureus* NDH-2 using the crystal structure of the monomer (4XDB) and distance restraints defining the dimer interface according to the *C. thermarum* NDH-2 dimer. The rationale for selecting this interface is based on the sequence alignment and the lack of the *S. cerevisiae* C-terminal dimerization helix in *S. aureus* NDH-2 (Fig. S4). Our SAXS-based structural model shows that a slightly twisted orientation of the monomers compared with the *C. thermarum* NDH-2 dimer results in an excellent agreement of the experimental and back-calculated SAXS data (Fig. 5C). Close inspection of the interface shows that the dimer is mainly stabilized by salt bridges (Fig. 5B). In the twisted dimeric structure, and in agreement with the homologous NDH-2 structures, the membrane attachment region is located at the same side of the dimer. Both helices including the conserved hydrophobic residues (F388, I393, and F397) are oriented parallel to the membrane and well-available for membrane binding (Fig. S4). Furthermore, to evaluate whether the conformation of the NDH-2 dimer could be different depending on the oxidation state of the enzyme, we performed SAXS analyses upon NADH reduction or quinone oxidation and is also maintained in the presence of 2-n-Heptyl-4-hydroxyquinoline-N-oxide (HQNO) or quinone alone (Table S1). Based on only minor differences in the SAXS data, we conclude that the oxidation state has only a minor or no effect on the dimerization and dimer orientation.

Given the lack of the *S. cerevisiae* Ndi1 C-terminal dimerization region in *S. aureus* NDH-2 and the observation that the dimer interface does not change in the presence of substrates we conclude that in solution NDH-2 adopts a conformation, which is slightly different to that of *C. thermarum* NDH-2 dimer structure rather than a conformational equilibrium between different conformations of the monomers.

Kinetics studies

Steady-state. Enzymatic activities were determined using DMN a menaquinone analogue, 2,3-Dimethoxy-5,6-dimethyl-benzoquinone (DDB) an ubiquinone analogue, or 2,3,5,6-Tetramethyl-1,4-benzoquinone (Duroquinone, DQ) a plastoquinone analogue as electron acceptors with NADH as the electron donor. The highest activities for the three tested quinones were obtained at 35°C (Fig. S5) is consistent with the optimum temperature of growth of *S. aureus*, which is 37°C.

Kcat values, obtained monitoring the consumption of NADH were $67.9 \pm 2.4\ s^{-1}$ for DMN, $69.4 \pm 2.3\ s^{-1}$ for DDB and $68.2 \pm 0.06\ s^{-1}$ for DQ.

The enzyme showed a Michaelis-Menten behavior toward NADH (using DMN as the electron acceptor), DMN, DDB and DQ (Fig. S6). V_{max} of 132.7 ± 6.6, 129.3 ± 4.6 and 119.1 ± 0.9 μmol NADH oxidized min^{-1} mg^{-1} of protein were obtained when using DMN, DDB or DQ as electron acceptor respectively. K_m values obtained for the three

quinones were similar to each other, 69.9 ± 6.4 μM for DMN, 63.7 ± 4.1 μM for DDB and 55.4 ± 0.5 μM for DQ. The K_m value for NADH was 20.5 ± 0.3 μM and V_{max} 175.9 ± 0.6 μmol NADH oxidized min^{-1} mg^{-1} of protein.

The presence of HQNO, a quinone derivative, already identified as a potent inhibitor of *S. cerevisiae* Ndi1 (Yamashita *et al*., 2007), was shown to decrease enzyme activity, regardless of the type of quinone used as substrate. A K_i app value of 6.8 ± 0.4 μM for HQNO was obtained when using DMN as electron acceptor (Fig. S7).

Fast kinetics. Upon addition of NADH to the oxidized NDH-2 (in a 1:1 ratio) spectral changes showed a very fast reduction of the enzyme, such that a significant part of the reaction is lost in the 3 ms dead time of the stopped-flow apparatus. The absorbance of the peak at 450 nm decreased and a broad band in the region 650–700 nm appeared (longer wavelength detection is limited by the diode array detector). Identical observed rate constants, 180 ± 30 s^{-1}, were obtained by fitting the kinetic traces acquired at 450 nm and at 670 nm to an exponential curve (Fig. 6A).

The spectral changes observed during the reduction of the enzyme were completely reversed when the NADH-reduced enzyme was mixed with DMN (1:1) (Fig. S8): the absorbance at 450 nm increased and the broad peak in the region 650–700 nm disappeared. The observed rate constants obtained by exponential fitting of the kinetic curves at 450 and 670 nm, were again identical and equal to 5.0 ± 0.5 s^{-1} (Fig. 6B). DDB and DQ were also tested, and the rate constants for the oxidation of the enzyme were of the same order of magnitude (Fig. S9).

Experiments allowing the enzyme to perform two turnovers were used to assess the effect of the inhibitor HQNO in the two half-reactions. NDH-2 plus DMN mixed with NADH was rapidly reduced, as observed by the drop in absorbance at 450 nm, and remained reduced while NADH was being oxidized, which was monitored by the decrease in absorbance at 350 nm (Fig. 6C–E). Upon NADH, exhaustion the enzyme was reoxidized by DMN (Fig. S10). The turnover rate determined from the decrease in absorbance at 350 nm was comparable with the rate at which the enzyme was reoxidized.

In the presence of HQNO the two half reactions were affected in a totally different manner: the rate of reduction of NDH-2 by NADH (1:2, protein : NADH), 364 ± 88 s^{-1}, was not significantly affected (considering that in this case the concentration of NADH present is the double) (Fig. 6C), the traces with and without inhibitor being superimposable in the 50 ms time scale. In the 0.75 s time scale, the reoxidation of the enzyme by DMN was only observed in the absence of the inhibitor, showing that the reoxidation of NDH-2 by DMN is strongly impaired in the presence of HQNO (Fig. 6D). To observe the reoxidation of NDH-2 by DMN in the presence of the inhibitor, it was necessary to acquire the signal in an even-longer time scale (75 s) (Fig. 6E). The rate of reoxidation of the enzyme by DMN slowed down by two orders of magnitude, 8 ± 2 s^{-1} *vs* 0.08 ± 0.02 s^{-1}, in the absence and presence of HQNO respectively.

Protein–substrate interaction

Fluorescence spectroscopy studies. NDH-2 from *S. aureus* has two tryptophan residues (W49 and W261). W261 is located at the *re* side of FAD and may interact with NADH (Heikal *et al*., 2014), whereas W49 is situated at the *si* side of FAD (Fig. S11). The fluorescence emission spectrum of NDH-2 with excitation at 280 nm exhibited the characteristics of a typical tryptophan fluorescence spectrum with a broad maximum at around 320–330 nm, whereas the fluorescence emission spectrum with excitation at 450 nm was typical of a flavoprotein, presenting a band with a maximum intensity at 530 nm. Only slight changes were observed in the region of the flavin fluorescence emission spectra in the presence of some ligands. By contrast, the intensity in the region of the tryptophan fluorescence emission spectra changed significantly and differently upon addition of each ligand.

When titrated independently with each quinone, DMN, DDB or DQ, a maximum decrease in tryptophan fluorescence between 80% and 90% was obtained (Fig. 7A and Fig. S12), while for NADH or NAD^+ this maximum was approximately 45% (Fig. 7B and Fig. S12), showing that the environment of the tryptophan residues is perturbed differently by the quinones and by NADH/NAD^+. The titration curve could be simulated using the equation of Monod-Wyman-Changeux (MWC) model for a dimeric enzyme, obtaining microscopic dissociation constants (K_s) of 11.4 μM for NADH and 20.3 μM for NAD^+ and 16.3, 19.1 and 25.8 μM for DMN, DDB and DQ respectively.

The maximum change in tryptophan fluorescence observed upon titration with HQNO was 20% (Fig. 7C), which suggests yet another mode of perturbation. NDH-2 was also titrated with NADH or DMN in the presence of HQNO. The titration profile of NDH-2 with NADH and HQNO is similar to that observed in the absence of HQNO (Fig. 7B); however, the titration profile with DMN in the presence of HQNO is different from that without HQNO (Fig. 7A). In fact, in the presence of HQNO, the titration profile with DMN could be fitted with a sigmoidal curve also using the equation of MWC model. The curve obtained in the presence of HQNO was simulated with K_S = 16.3 μM for DMN, the value obtained in the absence of HQNO.

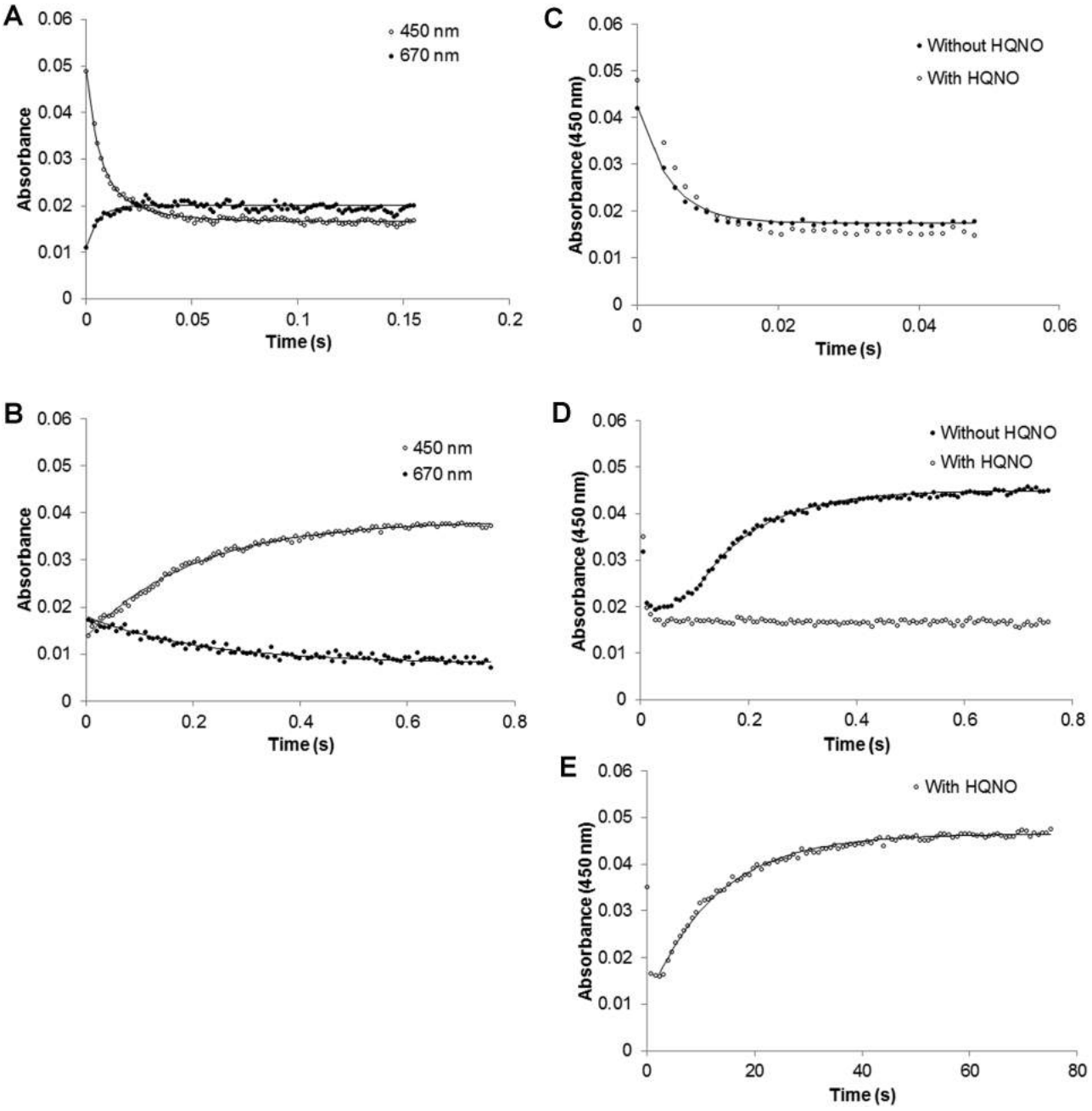

Fig. 6. Fast kinetics experiments.
A. Time-resolved reduction of NDH-2 from *S. aureus* by NADH (1:1, protein : NADH ratio). The absorbance of the peak at 450 nm decreases and a broad band appears in the region 650–700 nm. Identical rate constants, 180 ± 30 s^{-1}, were obtained by fitting the kinetic traces acquired at 450 nm and at 670 nm to an exponential curve.
B. Time-resolved oxidation of NDH-2 by DMN (1:1, protein : DMN ratio). The absorbance at 450 nm increased and the broad peak in the region 650–700 nm disappeared. The observed rate constants of the two processes, acquired at 450 nm and at 670 nm, obtained by exponential fitting of the kinetic curves at 450 and 670 nm, were identical and equal to 5 ± 0.5 s^{-1}.
C. Time-resolved reduction of NDH-2 by NADH in the presence and absence of the inhibitor, HQNO. The traces with and without inhibitor are superimposable in the 50 ms time scale.
D. In the 0.75 s time scale, the reoxidation of the enzyme by DMN is only observed in the absence of the inhibitor.
E. The reoxidation of NDH-2 by DMN in the presence of the inhibitor is observed when the signal is acquired in a longer time scale (75 s).
The values of the rate constants are the median of at least three independent experiments.

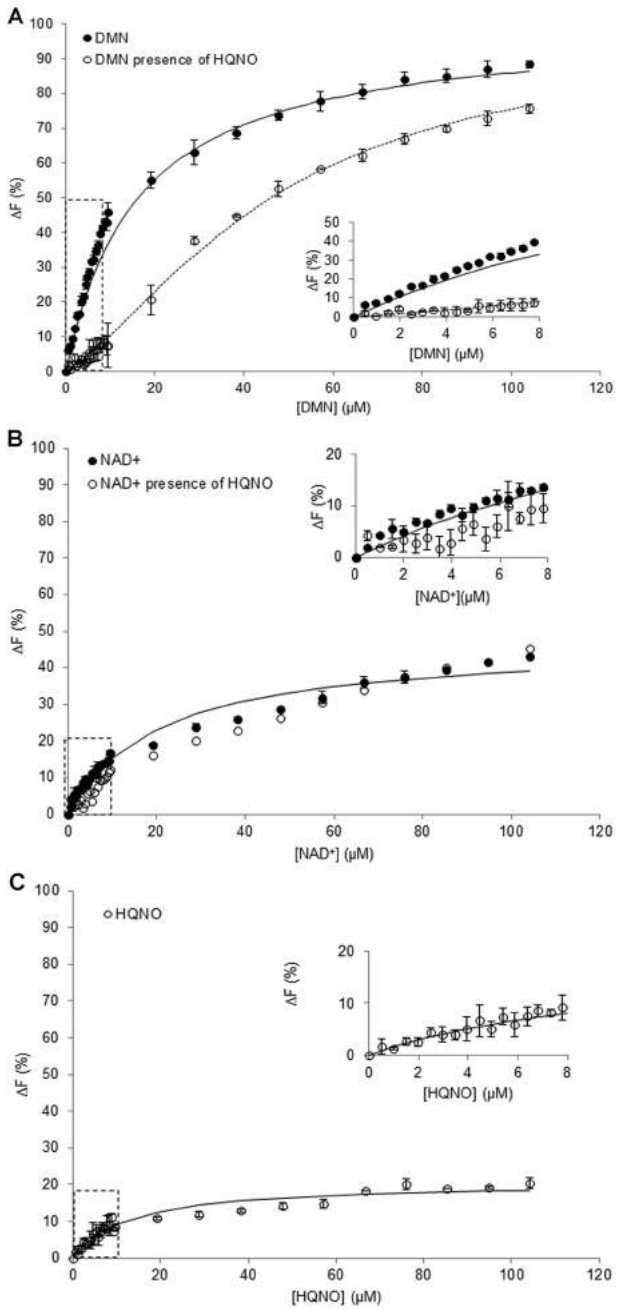

Fig. 7. Fluorescence spectroscopy.
A. Change in the fluorescence emission at 330 nm with excitation at 280 nm of NDH-2 by sequential addition of DMN or B. NAD^+ in the absence (closed circles) or in the presence of HQNO (open circles).
C. Change in the fluorescence emission at 330 nm with excitation at 280 nm of NDH-2 by sequential addition of HQNO. The curves were simulated with Monod-Wyman-Changeux (MWC) model equation, $\Delta F = \Delta F^{max} \times \frac{\frac{[S]}{K_s}\left(1+\frac{[S]}{K_s}\right)}{L+\left(1+\frac{[S]}{K_s}\right)^2}$, for a dimeric enzyme using $L = 0$ (no cooperativity), solid lines and $L = 7$ for the sigmoidal behavior, dashed line. The inserted figures expand the first measuring points at low concentration of DMN, NAD^+ or HQNO.

STD-NMR measurements. Protein ligand interactions were also investigated by saturation transfer difference (STD) NMR spectroscopy (Mayer and Meyer, 2001; Angulo *et al.*, 2010). In this case, the study of the interaction of different ligands with NDH-2 is monitored via the ligand by measuring the level of saturation transfer from the protein to the ligand when the protein is selectively saturated by magnetization. Initially the quinones, DMN, DDB and DQ were screened individually in the presence and in the absence of NDH-2, and clear STD-NMR signals were detected for the three quinones only in the presence of the protein. STD competition experiments revealed that DMN, DDB and DQ compete for the same binding site, indicating that their binding is specific (Fig. S13 and Table S2). Moreover, not all protons of DMN and DDB receive the same percentage of saturation (Table S2). For DMN, the STD spectrum (Fig. S13A) shows higher relative saturation percentages for the aromatic hydrogens (H2 and H3, close to 100%,) than for the methyl groups (H1, 87%) (Fig. S13A and Table S2). Also in the case of DDB the relative STD percentages determined for the protons of the methyl (H1, 87%) and methoxy groups (H2, 100%) are different (Fig. S13B and Table S2). These observations indicate a preferred orientation of DMN and DDB, with the contact with the protein occurring through the side of the aromatic ring in DMN and through the side of the methoxy groups in DDB.

To address the question of whether the two substrates, NADH and quinone, have the same binding site, the protein was titrated with NAD^+ in the presence of DMN and vice-versa. STD-NMR spectra were recorded for each condition and the STD amplification factor of DMN and NAD^+ were determined (Fig. 8A and B). NAD^+ was chosen instead of NADH to avoid the oxidoreduction reaction and the consequent disappearance of the NADH resonances and appearance of resonances assigned to NAD^+. Such situation would make the interpretation of the spectra much more complex. The STD amplification factors of DMN recorded in the absence or presence of a fixed concentration of NAD^+ were almost identical (Fig. 8A). Also in the presence of both compounds (DMN and NAD^+) the increase of DMN concentration had no effect on the STD amplification factor of NAD^+ (Fig. 8A). These results indicate that NAD^+ does not affect the binding of DMN to NDH-2. A similar behavior was observed on the reverse addition experiment upon increasing of NAD^+ concentration in the absence or presence of a fixed concentration of DMN; the STD amplification factor of NAD^+ increased with the increasing of NAD^+ in solution while the STD amplification factor of DMN did not change (Fig. 8B). These results clearly indicate the existence of different binding sites for NADH and quinone.

No STD effect was observed upon saturation of the protein in the presence of HQNO. This result can be

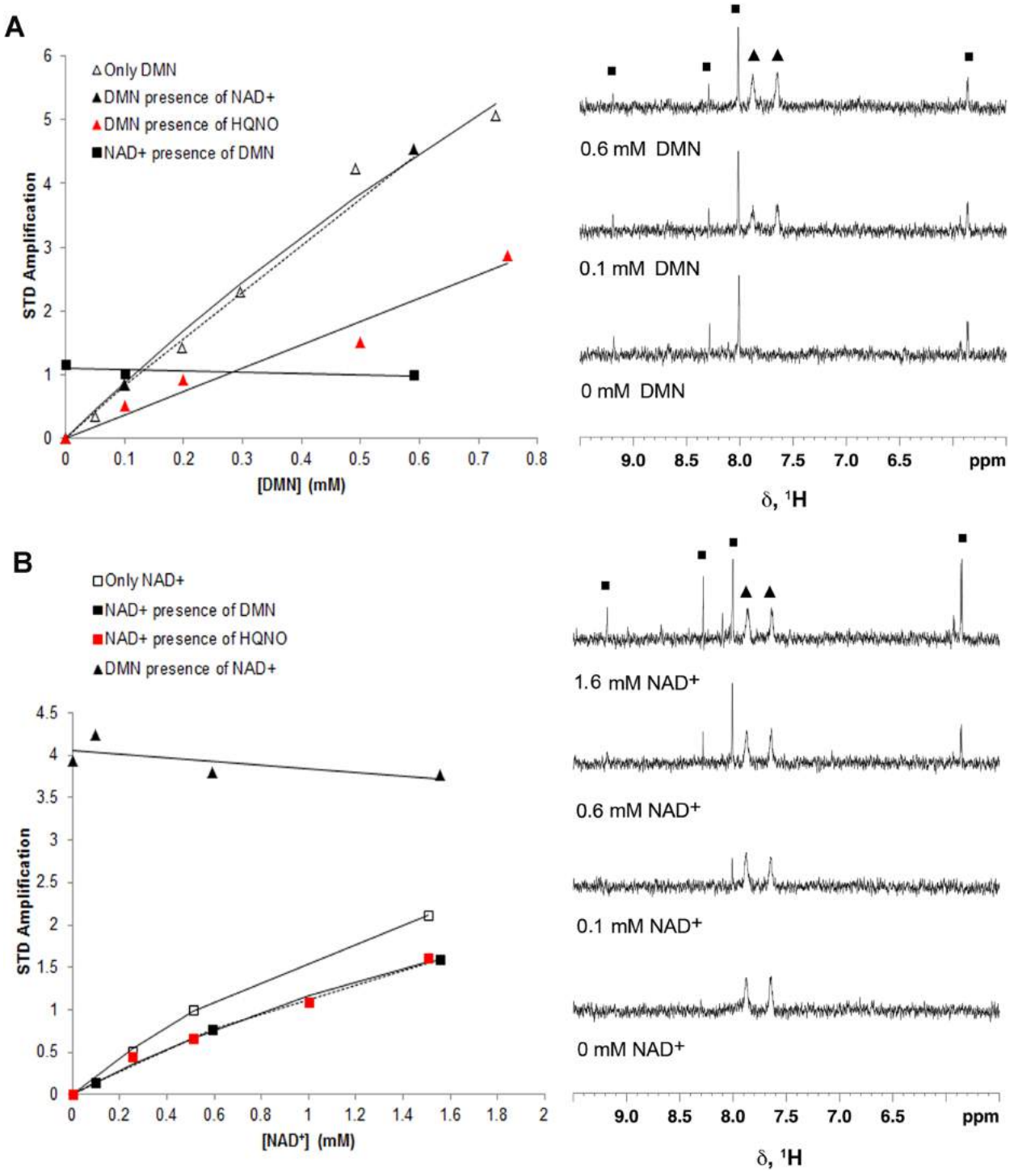

Fig. 8. STD-NMR Measurements.

A. Right – Plot of the STD amplification factor of DMN (from signal at 7.88 ppm) vs [DMN] measured in NDH-2 solutions titrated with DMN or in the presence of different compounds: only DMN (△, open triangle); DMN (▲, black closed triangle) in the presence of NAD^+, for which the NAD^+ amplification factor (from signal at 8 ppm) in the same sample was also measured (■, black closed square) and DMN (▲, red closed triangle) in the presence of HQNO. The curves are meant to be visual guide lines. Left – Illustrative STD-NMR spectra of NDH-2 titrated with DMN in the presence of NAD^+.

B. Right – Plot of the STD amplification factor of NAD^+ vs [NAD^+] measured in NDH-2 solutions titrated with NAD^+ in the presence of different compounds: only NAD^+ (□, open square); NAD^+ (■, black closed square) in the presence of DMN, for which the DMN amplification factor in the same sample was also measured (▲, black closed triangle), and NAD^+ in the presence of HQNO (■, red closed square). The curves are meant to be visual guide lines. Left – Illustrative STD-NMR spectra of NDH-2 titrated with NAD^+ in the presence of DMN.

interpreted as an absence of interaction between HQNO and the protein or as the occurrence of a strong interaction. Taking into account that the presence of HQNO affects the NADH:quinone oxidoreductase activity, a strong interaction between the protein and HQNO can be inferred. To check whether the HQNO effect is due to a possible binding to the quinone or to the NAD^+ site the variation of the STD amplification factor of DMN and NAD^+ were monitored as before, but in the presence of HQNO (Fig. S14). For DMN a substantial reduction of the STD amplification factor was observed when compared to the experiment in the absence of HQNO (Fig. 8A), but for NAD^+ the presence of HQNO had no significant effect on the profile of the STD amplification (Fig. 8B). These results also indicate that HQNO does not interfere with the NAD^+ binding and suggest a possible interaction with the quinone binding site. To check if the STD response of DMN could be completely suppressed by HQNO a STD experiment using a 15-fold excess of HQNO to DMN was performed. Even under these conditions the STD amplification factor was still similar to the one obtained with a 1:1 mixture of DMN and HQNO. Since the interaction of HQNO with the protein is stronger than that of DMN, this result is an indication that HQNO binds at a site which is close to that of DMN but not coincident with it.

Discussion

NDH-2 from *S. aureus* was expressed in *E. coli* and purified from the membranes. Its crystallographic structure was obtained being typical of the proteins of the flavin disulfide family containing NADH and FAD binding domains and in addition a membrane domain. Our SAXS measurements and size exclusion chromatography analysis showed that NDH-2 from *S. aureus* is a dimer in solution. The dimeric conformation seems not to change with the oxidation state of the enzyme.

We tested the activity and protein–substrate interaction using three different quinones, differing in their ring systems. DMN is a naphthoquinone characterized by its bicyclic ring system. DDB and DQ are benzoquinones thus presenting only one ring, which in the case of DDB contains two methoxy groups (Fig. S13). Besides their chemical differences, the three quinones also present distinct reduction potentials, –70 mV for DMN, 0 mV for DQ and 120 mV for DDB. We obtained similar activity and K_m values for the three quinones, which seem to reflect an absence of protein selectivity to different quinones. Similar activity values when using different quinones were also observed for NDH-2 from *M. tuberculosis* (Yano *et al*., 2014).

A long discussion has taken place about whether NADH and the quinone bind to the same or to different sites (Feng *et al*., 2012; Iwata *et al*., 2012). The crystal structures of the *S. cerevisiae* Ndi1 protein further stimulated this discussion, since that obtained by Iwata *et al*. (2012) suggests the same binding site for the two substrates, at the *re* side of the isoalloxazine ring system of FAD, whereas Feng *et al*. report different binding sites for NADH and quinone, at the *re* and *si* side of FAD respectively (Feng *et al*., 2012). Our crystal structure also suggests that NADH and the quinone bind to different sites. As already pointed out by Heikal *et al*., in order to the quinone to go around the isoalloxazine ring of FAD and interact with it from the *re* side, as suggested by Iwata *et al*., a considerable conformational change involving the membrane anchoring domain has to occur. Our fluorescence and STD data showed that indeed NADH and quinone bind to different sites. Furthermore, fluorescence and STD-NMR spectroscopic and fast kinetic data indicated that HQNO only interfered with the binding and reduction of the quinone. HQNO seemed not to affect the binding or oxidation of NADH. If the two substrates would bind to the same site, HQNO should affect both protein–substrate interaction for the two substrates and the respective half-reactions similarly. These differences indicate that NADH and quinone interact with the protein in distinct binding sites.

Fluorescence and STD-NMR spectroscopic data also reveal that HQNO interacts with the protein in a different way from those of NADH or DMN. The titration profile of HQNO and its maximum effect on tryptophan quenching or STD amplification factor are different from either NADH/NAD^+ or DMN. These observations, in addition to the result showing that the fluorescence titration profile of DMN is sigmoidal in the presence of HQNO, suggest that the inhibitor binds to a distinct site, stabilizing a conformation with less affinity for quinone, which is possibly also located at the *si*-side of the isoalloxazine ring of FAD as that of the quinone. In fact the existence of another quinone binding site has been already proposed (Feng *et al*., 2012; Yano *et al*., 2014), which would allow quinol to function as an allosteric activator (Yano *et al*., 2014).

Our fast kinetic measurements allowed the deconvolution of the two half-reactions. NADH oxidation occurs very fast, ~ 200 s^{-1} (for a stoichiometric reaction at 15°C), whereas quinone reduction is approximately 40 times slower. Furthermore, we observed that the enzyme is reduced during turnover (Fig. 6D, Fig. S10). Hence the rate limiting step of the reaction is the protein oxidation reaction by the quinone. Recently, Yano and co-workers suggested NADH oxidation as the reaction rate limiting step based on the observation that activity values were similar for high and low reduction potential quinones, i.e. that k_{cat} values were not simply a function of the midpoint reduction potential of each quinone (Yano *et al*., 2014). We have now observed that this is not the case.

Upon addition of the quinone to the NADH reduced enzyme (1:1), FAD is immediately oxidized as indicated by the appearance of absorption in the 370–450 region. Typical spectra indicating the presence of possible semiquinone forms of FAD were never observed, which suggests that FAD oxidation by the quinone is a two electron process.

The enzymatic reaction was previously proposed to have a ping-pong mechanism (Eschemann *et al*., 2005; Kerscher *et al*., 2008). Recently, such a mechanism and the possible existence of different binding sites for the substrate were reconciled by the proposal of a two-site ping-pong mechanism (Yano *et al*., 2014). In a ping-pong mechanism a ternary complex between the enzyme and its substrates/products is not formed. The recent work by Yano *et al*. (2014) differs from the previous report by Yang *et al*. (2011), who defended the establishment of a ternary complex based on the observation of a broad absorption band with maximum at 780 nm, which is characteristic of a charge transfer (CT) complex. This type of complex is frequently observed in flavoproteins, resulting from a $\pi - \pi$ interaction between the parallel stacked isoalloxazine and nicotinamide rings of reduced FAD and NAD^+ respectively (Sakurai and Hosoya, 1966). As reported by Yang et al. (2011), the CT band increased in intensity in the presence of electron acceptors, quinone or O_2 (Yang *et al*., 2011). We also observed the appearance of a broad absorption band in the 650–800 nm region, upon addition of NADH under anaerobic conditions and in the absence of quinone (Fig. 1A). Furthermore, we confirmed that the absorption in the 650–800 nm region is due to the establishment of a CT complex between the reduced flavin and NAD^+: upon reduction with dithionite the band in the 650–800 nm region did not appear, but was observed when NAD^+ was added (Fig. 1B). Our fast kinetic measurements also revealed that the reduction of the flavin is concomitant with the formation of the CT complex (Fig. 6 and Fig. S10). Furthermore, addition of quinone did not increase the intensity of the absorption band due to the CT complex, on the contrary, fast kinetic experiments showed that characteristic absorption bands of the flavin at 370–450 nm reappear and the CT band disappears upon addition of quinone, the oxidation of the flavin being simultaneous with the release of the CT complex. Although the reduction of FAD is independent on the presence of the quinone, the dissociation of the charge transfer complex, which indicates the release of NAD^+ (i.e. the release of the first product), is not. In a ping-pong mechanism NAD^+ would have to be released before quinone binding and this is not observed. The release of NAD^+ upon flavin oxidation by the quinone suggests the establishment of a ternary complex.

A similar behavior for reduction by NADH was described for the FAD-dependent reductase component of toluene dioxygenase (Lin *et al*., 2012). Based on both their kinetic and crystallographic studies, the authors suggested that the formation of the CT complex avoids reactivity with O_2, because the nicotinamide ring would shield the reactive C4a position of the flavin and force the isoalloxazine ring into a planar, less reactive conformation (Lin *et al*., 2012). NDH-2 is expressed under aerobic conditions and is a component of aerobic respiratory chains, thus a mechanism to prevent its reaction with O_2 would be most beneficial for the electron transfer chain.

Our work provides a thorough investigation of NDH-2, clearly showing that NDH-2 is a dimer in solution, has different binding sites for the two substrates, establishes a ternary complex during catalysis and that quinone reduction is the limiting reaction step. Quinone binding and reduction are affected by HQNO. This inhibition seems not to affect the binding nor the oxidation of NADH. Knowing that NDH-2 is the only enzyme with NADH:quinone oxidoreduction activity in many pathogenic organisms, including *S. aureus*, the work may also contribute to paving the way for rational design of novel antibiotics that target this enzyme.

Experimental procedures

Materials

2,3,5,6-Tetramethyl-1,4-benzoquinone (Duroquinone, DQ), NADH and NAD^+ were purchased from Sigma Aldrich. 2,3-Dimethoxy-5,6-dimethyl-p-benzoquinone (DDB) was acquired from Sequoia Research Products. 2,3-Dimethyl-1,4-naphthoquinone (DMN) was synthesized from menadione (Sigma Aldrich) (Kruber, 1929). 2-n-Heptyl-4-hydroxyquinoline-N-oxide (HQNO) was provided by Alexis Biochemicals and the Protease inhibitors cocktail tablets by Roche. BCA Protein Assay Reagent was purchased from Pierce; flavin adenine dinucleotide (FAD) was acquired from Merck and flavin mononucleotide (FMN) from Sigma Aldrich.

NDH-2 expression, purification and biochemical characterization

NDH-2 enzyme was cloned, expressed and purified as described in Rosario *et al*. (2015). Briefly, the gene SAOUHSC_00878, coding for the NDH-2 from *S. aureus* NCTC8325 was cloned into pET-28a(+) (Novagen) and expressed in *Escherichia coli* Rosetta 2 (DE3) pLysS cell strain. NDH-2 was purified from the membrane fraction washed with 2 M NaCl in two chromatographic steps, including a Q-sepharose and a Superdex 200 columns (GE Healthcare).

Protein concentration was determined by the BCA Protein Assay Reagent (Pierce) using BSA as standard. Protein purity was evaluated by SDS-PAGE and the protein was identified by mass spectrometry at the Unit MS, ITQB/IBET. The data was acquired in positive reflector MS and MS/MS modes in a 4800 *plus* MALDI-TOF/TOF (AB Sciex) mass

spectrometer, using 4000 Series Explorer Software v.3.5.3 (Applied Biosystems). External calibration was performed using Pepmix1 (Laser BioLabs).

The flavin prosthetic group was identified by reverse phase chromatography. The protein was denatured by incubation at 100°C for 10 min and removed by centrifugation. The supernatant was injected in a Waters, Nova Pack C18 60 Å 4 μm (3.9 × 150 mm) column operated in a Waters-Alliance HPLC system. The column was equilibrated with 100 mM ammonium acetate at pH 6 and 5% methanol (*V*/*V*) and the sample was eluted in the same buffer with a linear gradient from 5 to 15% methanol (*V*/*V*) at 1 ml min^{-1}. Commercial FAD and FMN were used as standards.

Flavin content of the pure protein was determined spectroscopically with a Shimadzu UV-1603 spectrophotometer, using the extinction coefficient of 11.3 mM^{-1} cm^{-1} at 450 nm for the free oxidized flavin. The extraction of FAD was done in the presence of 10% trichloroacetic acid (*V*/*V*) for 10 min followed by centrifugation for 15 min.

To investigate the oligomerization state of the protein size exclusion chromatography was performed using a Superdex 200 10/300 GL column (GE Healthcare) pre-equilibrated with 100 mM potassium phosphate, pH 7.0, 250 mM NaCl. Standards: Blue dextran, ferritin, aldolase, conalbumin, BSA and cytochrome *c* were used to obtain a calibration curve.

Thermal denaturation assays (25–90°C) were performed using a Peltier temperature controller with a rate of 0.5°C min^{-1}, and the data were recorded in intervals of 0.5°C with an acquisition time of 0.1 min. Denaturation was monitored by fluorescence spectroscopy using excitation at 450 nm and emission at 530 nm to monitor flavin fluorescence.

UV-Visible absorption spectroscopy was performed in an anaerobic chamber where 0.44 mg of NDH-2 was reduced by the addition of NADH or dithionite. When needed, a mixture of 5 mM glucose, 4 U ml^{-1} glucose oxidase and 130 U ml^{-1} catalase were used, to ensure total O_2-free conditions.

NDH-2 reduction potential was determined by cyclic voltammetry using a silver chloride (Ag/AgCl) electrode as the reference, graphite (Pg) as the working electrode and platinum (Pt), as the counter electrode. The electrolyte solution used was 100 mM potassium phosphate, pH 7.0 to ensure sufficient conductivity. Measurements were done with scan rates of 20 mV s^{-1}, 50 mV s^{-1}, 100 mV s^{-1}, 200 mV s^{-1}or 500 mV s^{-1} and data were then plotted as current (*i*) vs potential (*E*) to give the cyclic voltammogram trace.

Crystallization, data collection, structure determination and refinement

NDH-2 enzyme was crystallized as described in Rosario *et al*. (2015). Briefly, the first NDH-2 crystals were grown in 25% (w/V) PEG 3350 and 0.2 M sodium acetate pH 7.2, at 20°C, using 7 mg ml^{-1} of protein. As these crystals diffract poorly, streak seeding was successfully carried out yielding better quality crystals suitable for X-ray diffraction measurements (Rosario *et al*., 2015). Crystals were cryo-protected by transferring to a drop of solution 7 from the CryoProtX screen (Molecular Dimensions) and flash-frozen by quick plunging in liquid nitrogen.

A crystallographic dataset was collected at a wavelength of 0.873 Å to about 3 Å resolution on beamline ID23-2 of the European Synchrotron Radiation Facility (ESRF – Grenoble, France), from a single crystal. Crystals belong to the orthorhombic space group $P2_12_12_1$, with unit cell parameters a = 81.78, b = 86.03 and c = 269.95 Å, with $\alpha = \beta = \gamma = 90°$. Data were indexed and integrated using XDS (Kabsch, 2010), space group assignment was performed with POINTLESS (Evans, 2011) and scaling with SCALA/AIMLESS (Evans, 2006). All of these programs were used within the autoPROC (Vonrhein *et al*., 2011) data processing pipeline. An R_{free} flag was created at this stage corresponding to 5% of the measured reflections for this dataset.

The NDH-2 structure was solved by molecular replacement with PHASER (McCoy *et al*., 2007) using the bacterial *Caldalkalibacillus thermarum* (4NWZ), as search model and searching for four monomers in the asymmetric unit (corresponding to a Matthews coefficient (Matthews, 1968) of 2.64 $Å^3$ Da^{-1} and a solvent content of ~ 53%). The resulting PDB and MTZ files were fed into the AutoBuild wizard (Terwilliger *et al*., 2008) in PHENIX (Adams *et al*., 2002) for automated model building. The program built and docked to sequence 1483 residues belonging to four molecules in the asymmetric unit (a dimer of dimers, Fig. S2), with $R_{cryst}$of 20.5%, R_{free} of 24.6% and a map-model-correlation coefficient of 75% (Table 1). After an initial refinement carried out with BUSTER-TNT (Bricogne *et al*., 2011), clear electron density was observed for the FAD prosthetic group. Iterative manual model building and refinement were carried out in a cyclic manner with COOT (Emsley *et al*., 2010) and phenix.refine (Afonine *et al*., 2012), until a complete model was built and refinement convergence achieved. The stereochemistry of the refined model and the Ramachandran plot were assessed with MolProbity (Chen *et al*., 2010). The model comprises 95.1%, 4.1% and 0.8% of the residues in the favored, allowed and disallowed regions of the Ramachandran respectively. Structure representations were rendered with PyMOL (The PyMOL Molecular Graphics System, Version 1.5.0.4 Schrödinger, LLC). Electrostatic surface potentials were calculated with APBS (Baker *et al*., 2001) after generating PQR input files with the online PDB2PQR server (Dolinsky *et al*., 2004). The co-ordinates and structure factor amplitudes of *S. aureus* NDH-2 have been deposited in the Protein Data Bank under the accession number 4XDB.

Small-angle X-ray Scattering measurements and data analysis

SAXS data for NDH-2 from *S. aureus* in solution were recorded on an in-house SAXS instrument (SAXSess mc2, Anton Paar, Graz, Austria) equipped with a Kratky camera, a sealed X-ray tube source and a two-dimensional Princeton Instruments PI•SCX:4300 (Roper Scientific) CCD detector. The scattering patterns were measured with a 180 min exposure time (1080 frames, each 10 s) for several protein concentrations in the range from 0.6 to 8.0 mg ml^{-1}. For the measurement of ligand-bound states, 35 μM NDH-2 was mixed with a three times stoichiometric excess of DMN, HQNO, DMN/HQNO, NAD^+, and NADH respectively. Radiation damage was excluded based on a comparison of individual frames of the 180 min exposures, where no changes were detected. A range of momentum transfer of $0.012 < s < 0.63$ $Å^{-1}$ was covered ($s = 4\pi \sin(\theta)/\lambda$, where 2θ is

the scattering angle and $\lambda = 1.5$ Å is the X-ray wavelength). All SAXS data were analyzed with the package ATSAS (version 2.5 EMBL Hamburg, Hamburg, Germany). The data were processed with the SAXSQuant software (version 3.9 Anton Paar GmbH, Graz, Austria) and desmeared using the programs GNOM (Svergun, 1992) and GIFT (Bergmann *et al*., 2000). The forward scattering, I(0), the radius of gyration, R_g, the maximum dimension, D_{max}, and the inter-atomic distance distribution functions, (P(R)), were computed with the program GNOM. The masses of the protein were evaluated by comparison of the forward scattering intensity with that of a human serum albumin reference solution (molecular mass 69 kDa) and using Porod's law. SAXS data were back-calculated for NDH-2 from *C. thermarum* (4NWZ) and *S. cerevisiae* Ndi1 (4G9K) using the program CRYSOL (EMBL Hamburg, Hamburg, Germany) (Svergun *et al*., 1995) and taken as input for population analysis. The solution structures of dimeric *S. aureus* were modeled using the program CORAL (EMBL Hamburg, Hamburg, Germany) (Petoukhov *et al*., 2012). Input were the crystal structure of *S. aureus* determined here, SAXS data, and maximal Cα-Cα distance restraints loosely defining the dimer interface based on that of the crystal structure of NDH-2 from *C. thermarum* (4NWZ; Ile132-Ala149 15.9 Å, Thr133-Ala150 17.2 Å, Arg 135-Ala146 15.6 Å, Glu136-Asn147 15.4 Å, Arg139-Glu142 16.4 Å, His140-His140 18.5 Å, His140-Asp143 16.0 Å, Asp143-Asp143 16.8 Å; all distances are the distances of the aligning residues in 4NWZ plus an additional tolerance of 10 Å). Throughout the calculations, the 5 N-terminal residues were defined flexible and randomized. A total of 50 structures were calculated, and the best structures based on the fit to the experimental data selected to prepare the figures.

Steady-state kinetics

Activity assays were performed on a Shimadzu UV-1800 spectrophotometer monitoring the change in absorbance of the electron donor, NADH, at 340 nm. The reaction mixture (1000 µl) contained 20 nM NDH-2 in 100 mM potassium phosphate pH 7.0, 250 mM NaCl. The activity assays were made inside an anaerobic chamber at 35°C, using as electron acceptors DMN, DDB or DQ. The applied quinone concentrations were in the range from 5 to 200 µM (at 100 µM NADH) and the NADH concentrations were in the range from 5 to 150 µM (at 150 µM DMN). HQNO was added in the range from 1 to 100 µM.

The NADH extinction coefficient of 6.22 mM^{-1} cm^{-1} was used to calculate NDH-2 specific activity (µmol^{-1} min^{-1} mg protein). Data were fitted by the Michaelis-Menten equation, $v_0 = \frac{v_{max}[S]}{K_m + [S]}$ using a non-linear least-squares regression to determine K_m and V_{max} values for the reactions with NADH and with DMN, DDB or DQ. All the values were obtained from three independent assays. The equilibrium dissociation constant for the inhibitor was obtained using the equation $v_0^i = v_0^{max} \frac{\left(1+\beta\frac{[I]}{K_i^{app}}\right)}{\left(1+\frac{[I]}{K_i^{app}}\right)}$. The activity temperature profile study was performed at pH 7.0 and between 20 and 55°C.

Fast kinetics experiments

The transient kinetics of reduction of NDH-2 by NADH and oxidation of reduced NDH-2 by quinone were studied by stopped-flow using a TGK Scientific SF-61 DX2 apparatus placed inside an anaerobic chamber MBraun 130 with an oxygen level below 1 ppm. The temperature of the drive syringes and mixing chamber was maintained at 15°C, and the pH was controlled with 100 mM potassium phosphate pH 7.0, 250 mM NaCl. All solutions were prepared inside the anaerobic chamber with degassed water. The time course of the reactions was monitored with a photodiode array (350–700 nm).

For the study of the reductive half-reaction, 10 µM oxidized NDH-2 was mixed with 10 µM NADH (1:1 ratio). To follow the time evolution of the reduction of the protein 100 spectra were acquired in 150 ms. The rate constant was obtained from the fitting of the kinetic traces recorded at the wavelengths at which spectral changes were most evident (in this case at 450 nm and 670 nm). As a significant part of the signal is lost in the dead time of the apparatus (even at 15°C), the absorbance at time zero was taken from a control experiment where NDH-2 was mixed with buffer. The time scale was corrected for the dead time (3 ms), and the fit of an exponential curve to the data was performed with the tool *solver* from Microsoft Office Excel program.

For the study of the oxidative half-reaction, 10 µM NDH-2 was reduced with a stoichiometric amount of NADH and the reduced state of the enzyme checked in a control experiment against buffer. Reduced NDH-2 was then mixed with 10 µM DMN in a 1:1 ratio. The software Kinetic Studio from TGK was used to fit exponential curves to the kinetic traces acquired at 450 nm and 670 nm. The values of the rate constants presented are the median of at least three independent experiments.

The effect of the inhibitor HQNO was tested in experiments in which the enzyme was allowed to complete two turnovers. Control experiments were performed with 10 µM NDH-2 plus 30 µM DMN mixed with 20 µM NADH. In the experiments with inhibitor, 50 µM HQNO was added to the syringe containing the enzyme and DMN, before mixing it with NADH in the stopped-flow apparatus.

Fluorescence quenching studies

Fluorescence spectra were obtained on a Varian Cary Eclipse spectrofluorimeter. The reaction mixture (500 µl) contained 2 µM NDH-2 in 100 mM potassium phosphate pH 7.0 and 250 mM NaCl. The effect of NADH, NAD^+, DMN, DDB, DQ or HQNO was tested. Three independent titrations were performed with each ligand in the range of 0 to 100 µM. Fluorescence emission spectra of each ligand, with excitation at 280 nm or 450 nm, were recorded as controls.

Tryptophan and flavin fluorescence emission spectra were recorded at 25°C with excitation wavelengths at 280 nm and 450 nm respectively. The change in emission at 330 nm (ΔF) was normalized and plotted *vs* ligand concentration. At the end of each titration, a thermal denaturation assay was performed to evaluate protein stability. The

equation of Monod-Wyman-Changeux (MWC) model, $\Delta F = \Delta F^{max} \times \frac{\frac{[S]}{K_s}\left(1+\frac{[S]}{K_s}\right)}{L+\left(1+\frac{[S]}{K_s}\right)^2}$ for a dimeric enzyme was used to simulate the data.

Saturation transfer difference (STD) NMR

NMR spectra were acquired in a Bruker Avance III spectrometer at 15°C, operating at a proton frequency of 600.13 MHz with a 5 mm triple resonance cryogenic probe head. STD-NMR spectra were acquired with 1024 transients in a matrix with 32 k data points in t2 in a spectral window of 12019.23 Hz centered at 2814.60 Hz. Excitation sculpting with gradients was employed to suppress the water proton signals. Selective saturation of protein resonances (on resonance spectrum) was performed by irradiating at –300 Hz using a series of 40 Eburp2.1000 shaped 90° pulses (50 ms, 1 ms delay between pulses), for a total saturation time of 2.0 s. For the reference spectrum (off resonance), the samples were irradiated at 20000 Hz. Control experiments were performed with the reference samples in order to optimize the frequency for protein saturation (–0.5 ppm) and off-resonance irradiation to ensure that none of the tested ligands would be saturated at this frequency. STD spectra were obtained by subtraction of the off resonance and the on resonance spectra. The STD effect was calculated by $(I_0–I_{STD})/I_0$, in which $(I_0–I_{STD})$ is the peak intensity in the STD spectrum and I_0 is the peak intensity in the off resonance spectrum. STD amplification factors were calculated by multiplying the STD effect by the ligand protein ratio. For epitope mapping the STD intensity of the largest STD effect was set to 100% as a reference, and the relative intensities were determined. Relative STD-NMR values for the experiments of NDH-2 with DMN, DDB or DQ and for the STD competition experiments were obtained from at least three independent assays.

The STD-NMR experiments were performed with NDH-2 in 100 mM potassium phosphate pH 7.0 (prepared in D_2O) and 250 mM NaCl buffer and the different ligands NADH, NAD^+, DMN, DDB, DQ or HQNO in the buffer with 10% DMSO. The final concentrations of protein and ligands were 10 μM and 0.5 mM respectively.

Acknowledgements

We acknowledge David L. Turner for the critical reading of the manuscript, Ana Lúcia Rosário for the initial crystallization trials and optimization, Smilja Todorovic and Célia Silveira for CV measurements, João Carita for cell growth, Paula Chicau for HPLC analysis of the flavin and Afonso Duarte and Bruno C. Marreiros for discussions. The NMR spectrometers are part of The Portuguese National NMR Facility, supported by Fundação para a Ciência e a Tecnologia (RECI/BBB-BQB/0230/2012), and the stopped-flow apparatus was purchased by the grant REEQ/336/BIO/2005 from Fundação para a Ciência e a Tecnologia. A.P.B. and J.A.B are recipients of grants SFRH/BPD/80741/2011 and SFRH/BPD/79224/2011, respectively, from Fundação para a Ciência e a Tecnologia. T.M. was supported by the Bavarian Ministry of Sciences, Research and the Arts (Bavarian Molecular Biosystems Research Network, to T.M.), the German Research Foundation (Emmy Noether program MA 5703/1-1, to T.M.), the Centre for Integrated Protein Science Munich (CIPSM), the President's International Fellowship Initiative of CAS (No:2015VBB045, to T.M.) and the National Natural Science Foundation of China (No. 31450110423, to T.M.). The authors acknowledge the Leibniz Supercomputing Centre (LRZ, http://www.lrz.de) for providing computing time on the Linux Cluster. M. M. P. and E. J. C. acknowledge networking support by the COST Action CM1306 – Understanding Movement and Mechanism in Molecular Machines. The project was funded by Fundação para a Ciência e a Tecnologia (PTDC/BBB-BQB/2294/2012 to M.M.P.). The work was supported by Fundação para a Ciência e a Tecnologia through Grant # PEst-OE/EQB/LA0004/2011. The authors have no conflict of interest to declare.

References

Adams, P.D., Grosse-Kunstleve, R.W., Hung, L.W., Ioerger, T.R., McCoy, A.J., Moriarty, N.W., *et al.* (2002) PHENIX: building new software for automated crystallographic structure determination. *Acta Crystallogr D Biol Crystallogr* **58:** 1948–1954.

Afonine, P.V., Grosse-Kunstleve, R.W., Echols, N., Headd, J.J., Moriarty, N.W., Mustyakimov, M., *et al.* (2012) Towards automated crystallographic structure refinement with phenix.refine. *Acta Crystallogr D Biol Crystallogr* **68:** 352–367.

Angulo, J., Enriquez-Navas, P.M., and Nieto, P.M. (2010) Ligand-receptor binding affinities from saturation transfer difference (STD) NMR spectroscopy: the binding isotherm of STD initial growth rates. *Chemistry (Easton)* **16:** 7803–7812.

Baker, N.A., Sept, D., Joseph, S., Holst, M.J., and McCammon, J.A. (2001) Electrostatics of nanosystems: application to microtubules and the ribosome. *Proc Natl Acad Sci USA* **98:** 10037–10041.

Bergmann, A., Fritz, G., and Glatter, O. (2000) Solving the generalized indirect Fourier transformation (GIFT) by Boltzmann simplex simulated annealing (BSSA). *J Appl Crystallogr* **33:** 1212–1216.

Biagini, G.A., Fisher, N., Shone, A.E., Mubaraki, M.A., Srivastava, A., Hill, A., *et al.* (2012) Generation of quinolone antimalarials targeting the *Plasmodium falciparum* mitochondrial respiratory chain for the treatment and prophylaxis of malaria. *Proc Natl Acad Sci USA* **109:** 8298–8303.

Bricogne, G., Blanc, E., Brandl, M., Flensburg, C., Keller, P., Paciorek, W., *et al.* (2011) BUSTER version 2.10. Cambridge, United Kingdom: Global Phasing Ltd.

Brito, J.A., Sousa, F.L., Stelter, M., Bandeiras, T.M., Vonrhein, C., Teixeira, M., *et al.* (2009) Structural and functional insights into sulfide:quinone oxidoreductase. *Biochemistry* **48:** 5613–5622.

Brumfitt, W., and Hamilton-Miller, J.M. (1990) The worldwide problem of methicillin-resistant *Staphylococcus aureus*. *Drugs Exp Clin Res* **16:** 205–214.

Chen, V.B., Arendall, W.B., 3rd, Headd, J.J., Keedy, D.A.,

Immormino, R.M., Kapral, G.J., *et al*. (2010) MolProbity: all-atom structure validation for macromolecular crystallography. *Acta Crystallogr D Biol Crystallogr* **66:** 12–21.
Cherney, M.M., Zhang, Y., James, M.N., and Weiner, J.H. (2012) Structure-activity characterization of sulfide:quinone oxidoreductase variants. *J Struct Biol* **178:** 319–328.
Cook, G.M., Greening, C., Hards, K., and Berney, M. (2014) Energetics of pathogenic bacteria and opportunities for drug development. *Adv Microb Physiol* **65:** 1–62.
Dawson, T.M., and Dawson, V.L. (2003) Molecular pathways of neurodegeneration in Parkinson's disease. *Science* **302:** 819–822.
Dolinsky, T.J., Nielsen, J.E., McCammon, J.A., and Baker, N.A. (2004) PDB2PQR: an automated pipeline for the setup of Poisson-Boltzmann electrostatics calculations. *Nucleic Acids Res* **32:** W665–W667.
Edwards, A.M. (2014) *Flavins and Flavoproteins: Methods and Protocols*, Vol. 1146. New York: Springer Science.
Emsley, P., Lohkamp, B., Scott, W.G., and Cowtan, K. (2010) Features and development of Coot. *Acta Crystallogr D Biol Crystallogr* **66:** 486–501.
Eschemann, A., Galkin, A., Oettmeier, W., Brandt, U., and Kerscher, S. (2005) HDQ (1-hydroxy-2-dodecyl-4(1H)quinolone), a high affinity inhibitor for mitochondrial alternative NADH dehydrogenase: evidence for a ping-pong mechanism. *J Biol Chem* **280:** 3138–3142.
Evans, P. (2006) Scaling and assessment of data quality. *Acta Crystallogr D Biol Crystallogr* **62:** 72–82.
Evans, P.R. (2011) An introduction to data reduction: space-group determination, scaling and intensity statistics. *Acta Crystallogr D Biol Crystallogr* **67:** 282–292.
Farha, M.A., Verschoor, C.P., Bowdish, D., and Brown, E.D. (2013) Collapsing the proton motive force to identify synergistic combinations against *Staphylococcus aureus*. *Chemistry & Biology* **20:** 1168–1178.
Feng, Y., Li, W., Li, J., Wang, J., Ge, J., Xu, D., *et al*. (2012) Structural insight into the type-II mitochondrial NADH dehydrogenases. *Nature* **491:** 478–482.
Heikal, A., Nakatani, Y., Dunn, E., Weimar, M.R., Day, C.L., Baker, E.N., *et al*. (2014) Structure of the bacterial type II NADH dehydrogenase: a monotopic membrane protein with an essential role in energy generation. *Mol Microbiol* **91:** 950–964.
Iwata, M., Lee, Y., Yamashita, T., Yagi, T., Iwata, S., Cameron, A.D., *et al*. (2012) The structure of the yeast NADH dehydrogenase (Ndi1) reveals overlapping binding sites for water- and lipid-soluble substrates. *Proc Natl Acad Sci USA* **109:** 15247–15252.
Kabsch, W. (2010) Xds. *Acta Crystallogr D Biol Crystallogr* **66:** 125–132.
Kerscher, S., Drose, S., Zickermann, V., and Brandt, U. (2008) The three families of respiratory NADH dehydrogenases. *Results Probl Cell Differ* **45:** 185–222.
Kerscher, S.J. (2000) Diversity and origin of alternative NADH:ubiquinone oxidoreductases. *Biochim Biophys Acta* **1459:** 274–283.
Krissinel, E., and Henrick, K. (2007) Inference of macromolecular assemblies from crystalline state. *J Mol Biol* **372:** 774–797.
Kruber, O. (1929) 0. Kruber: Über das 2.3-Dimethylnaphthalin im Steinkohlenteer. *Jahrg* **62:** 3044–3047.
Lin, S.S., Gross, U., and Bohne, W. (2011) Two internal type II NADH dehydrogenases of *Toxoplasma gondii* are both required for optimal tachyzoite growth. *Mol Microbiol* **82:** 209–221.
Lin, T.Y., Werther, T., Jeoung, J.H., and Dobbek, H. (2012) Suppression of electron transfer to dioxygen by charge transfer and electron transfer complexes in the FAD-dependent reductase component of toluene dioxygenase. *J Biol Chem* **287:** 38338–38346.
McCoy, A.J., Grosse-Kunstleve, R.W., Adams, P.D., Winn, M.D., Storoni, L.C., and Read, R.J. (2007) Phaser crystallographic software. *J Appl Crystallogr* **40:** 658–674.
Marcia, M., Ermler, U., Peng, G., and Michel, H. (2009) The structure of *Aquifex aeolicus* sulfide:quinone oxidoreductase, a basis to understand sulfide detoxification and respiration. *Proc Natl Acad Sci USA* **106:** 9625–9630.
Matthews, B.W. (1968) Solvent content of protein crystals. *J Mol Biol* **33:** 491–497.
Mayer, M., and Meyer, B. (2001) Group epitope mapping by saturation transfer difference NMR to identify segments of a ligand in direct contact with a protein receptor. *J Am Chem Soc* **123:** 6108–6117.
Petoukhov, M.V., Franke, D., Shkumatov, A.V., Tria, G., Kikhney, A.G., Gajda, M., *et al*. (2012) New developments in the program package for small-angle scattering data analysis. *J Appl Crystallogr* **45:** 342–350.
Rosario, A.L., Sena, F.V., Batista, A.P., Oliveira, T.F., Athayde, D., Pereira, M.M., *et al*. (2015) Expression, purification, crystallization and preliminary X-ray diffraction analysis of a type II NADH:quinone oxidoreductase from the human pathogen *Staphylococcus aureus*. *Acta Crystallographica Section F, Structural biology communications* **71:** 477–482.
Sakurai, T., and Hosoya, H. (1966) Charge-transfer complexes of nicotinamide-adenine dinucleotide analogues and flavin mononucleotide. *Bibl Laeger* **112:** 459–468.
Salgado-Pabon, W., and Schlievert, P.M. (2014) Models matter: the search for an effective *Staphylococcus aureus* vaccine. *Nat Rev Microbiol* **12:** 585–591.
Schapira, A.H. (1998) Mitochondrial dysfunction in neurodegenerative disorders. *Biochim Biophys Acta* **1366:** 225–233.
Schurig-Briccio, L.A., Yano, T., Rubin, H., and Gennis, R.B. (2014) Characterization of the type 2 NADH:menaquinone oxidoreductases from *Staphylococcus aureus* and the bactericidal action of phenothiazines. *Biochim Biophys Acta* **1837:** 954–963.
Svergun, D., Barberato, C., and Koch, M.H.J. (1995) CRYSOL – a program to evaluate x-ray solution scattering of biological macromolecules from atomic coordinates. *J Appl Crystallogr* **28:** 768–773.
Svergun, D.I. (1992) Determination of the regularization parameter in indirect-transform methods using perceptual criteria. *J Appl Crystallogr* **25:** 495–503.
Terwilliger, T.C., Grosse-Kunstleve, R.W., Afonine, P.V., Moriarty, N.W., Zwart, P.H., Hung, L.W., *et al*. (2008) Iterative model building, structure refinement and density modification with the PHENIX AutoBuild wizard. *Acta Crystallogr D Biol Crystallogr* **64:** 61–69.
Velazquez, I., and Pardo, J.P. (2001) Kinetic characterization of the rotenone-insensitive internal NADH: ubiquinone oxi-

doreductase of mitochondria from *Saccharomyces cerevisiae*. *Arch Biochem Biophys* **389:** 7–14.
Vonrhein, C., Flensburg, C., Keller, P., Sharff, A., Smart, O., Paciorek, W., *et al*. (2011) Data processing and analysis with the autoPROC toolbox. *Acta Crystallogr D Biol Crystallogr* **67:** 293–302.
Weinstein, E.A., Yano, T., Li, L.S., Avarbock, D., Avarbock, A., Helm, D., *et al*. (2005) Inhibitors of type II NADH:menaquinone oxidoreductase represent a class of antitubercular drugs. *Proc Natl Acad Sci USA* **102:** 4548–4553.
Yagi, T., Seo, B.B., Nakamaru-Ogiso, E., Marella, M., Barber-Singh, J., Yamashita, T., *et al*. (2006) Can a single subunit yeast NADH dehydrogenase (Ndi1) remedy diseases caused by respiratory complex I defects? *Rejuvenation Res* **9:** 191–197.
Yamashita, T., Nakamaru-Ogiso, E., Miyoshi, H., Matsuno-Yagi, A., and Yagi, T. (2007) Roles of bound quinone in the single subunit NADH-quinone oxidoreductase (Ndi1) from *Saccharomyces cerevisiae*. *J Biol Chem* **282:** 6012–6020.
Yang, Y., Yamashita, T., Nakamaru-Ogiso, E., Hashimoto, T., Murai, M., Igarashi, J., *et al*. (2011) Reaction mechanism of single subunit NADH-ubiquinone oxidoreductase (Ndi1) from *Saccharomyces cerevisiae*: evidence for a ternary complex mechanism. *J Biol Chem* **286:** 9287–9297.
Yano, T., Li, L.S., Weinstein, E., Teh, J.S., and Rubin, H. (2006) Steady-state kinetics and inhibitory action of antitubercular phenothiazines on *mycobacterium tuberculosis* type-II NADH-menaquinone oxidoreductase (NDH-2). *J Biol Chem* **281:** 11456–11463.
Yano, T., Rahimian, M., Aneja, K.K., Schechter, N.M., Rubin, H., and Scott, C.P. (2014) *Mycobacterium tuberculosis* type II NADH-menaquinone oxidoreductase catalyzes electron transfer through a two-site ping-pong mechanism and has two quinone-binding sites. *Biochemistry* **53:** 1179–1190.

Supporting information

Additional supporting information may be found in the online version of this article at the publisher's web-site.